 doi:10.20944/preprints201907.0028.v1

Article

Comparative Study Of The Reactivity Of The Tungsten Oxides WO_2 And WO_3 With Beryllium At Temperatures Up To 1273 K

Martin Köppen [1]*

[1] Independent researcher, Gabelsbergerstr. 9, 94032 Passau, Germany; martin_koeppen@gmx.de

Abstract: Tungsten oxides play a pivotal role in a variety of modern devices e.g. switchable glasses, wastewater treatment and modern gas sensors and metallic tungsten is used as armour material for e.g. gas turbines and future fusion power devices. In the first case you want to keep the oxide as functional material, while in the second case oxides can lead to catastrophic failures and you want avoid oxidation of tungsten. In both cases it is crucial to understand the stability of the tungsten oxides against chemicals. In this study the different reactivity of tungsten oxides towards the highly oxophilic beryllium is studied and compared. Tungsten–(IV)–oxide and tungsten–(VI)–oxide layers are prepared on a tungsten substrate. In the next step a thin film of beryllium is evaporated on the samples. In consecutive steps the sample is heated in steps of 100 K from r. t. to 1273 K. The chemical composition is investigated after each experimental step by high resolution X–ray photoelectron spectroscopy (XPS) of all involved core levels as well as the valence bands. A model is developed to analyse the chemical reactions after each step. In this study, we found the tungsten trioxid is reduced already by beryllium at r. t. and starts to react towards the ternary compounds $BeWO_3$ and $BeWO_4$ at temperatures starting from 673 K. However, tungsten dioxide is reduction resistant to temperatures up to 1173 K. In conclusion, we found the WO_2 surface to be much more chemical resistant towards the reduction agent Be than WO_3.

Keywords: x–ray photoelectron spectroscopy; physical vapor deposition; x–ray diffraction; tungsten oxide; tungsten dioxide; tungsten trioxide; beryllium; tungstate; tungsten bronze;

1. Introduction

Tungsten and its oxides play a pivotal role for the solution of recent material problems. Tungsten oxides have lately received a lot of attention. In consumer electronics they are used in switchable glass due to its electrochromic properties. [1–3] In wastewater treatment tungsten oxides are used as catalysts. [4] Modern gas sensors rely on tungsten oxides. [5–7] All these application have in common, that the stability of tungsten oxides is desirable.

A more classic way to use tungsten is in high heat load environments, like turbines or reactors. Here the oxidation of tungsten has catastrophic effects. The reduction of the melting point from approx. 3600 K to approx. 1700 K is severe and eventually leads to failure of the respective components.

In material research for future fusion reactors, tungsten oxides are adverse in a second way: The formation of tungsten oxide is a severe safety issue. Tungsten trioxide is under the conditions in a fusion reactor volatile. Due to the neutron radiation from the D–T fusion reaction, tungsten can be transmutated into its radioactive isotopes. The formation of volatile tungsten oxides leads therefore to mobilised radioactivity, which is unfavourable.

In both cases an investigation of the stability of the different oxides is crucial. This study aims to investigate the stability of thin layers of ceramic tungsten trioxide as well as a thin layer of its metallic counter part, tungsten dioxide. In this study we will evaporate a thin layer of highly oxophilic beryllium and investigate the composition by X–ray photoelectron spectroscopy. Successively, we increase the temperature in 100 K steps up to a final temperature of 1273 K. After each

 doi:10.20944/preprints201907.0028.v1

step the composition is investigated anew. This approach allows us to make predictions about the thermochemical stability.

2. Experimental

All XPS–measurements are carried out with a *PHI 5600 ESCA* X–ray photoelectron spectroscopy system equipped with a monochromatic Al K_α X–ray source and a hemispherical energy analyser. The analysis chamber is directly connected to a preparation chamber with an electron beam evaporator equipped with beryllium and a sample heater. Base pressures in both chambers is in the range of $1 \cdot 10^{-10}$ hPa. For the complete experimental setup, see refs. [8–10].

The tungsten trioxide is synthesised in an external oven under air. A tungsten plate (1 cm^2) is heated for one hour at 773 K. The XP–spectrum shows signal contributions of 88.2 % WO_3 and 11.8 % of its surface compound $WO_2(OH)_2$.

As precursor for the tungsten dioxide a tungsten plate of the same size is heated in the same oven flushed with nitrogen at 1000 hPa overpressure under air. The educt is heated for 15 min at 673 K resulting in a thin WO_3–layer. The precursor is introduced into the analysis chamber. It is converted into WO_2 in a comproportioning reaction at 973 K for one hour. The XP–spectrum shows a signal contribution of 41.41 % WO_2. The rest of the signal consists of 30.81 % WO_{3-x}, 25.44 % WO_3 and 2.33 % W as byproducts. This results in a yield of 27.61 % and a selectivity of 28.27 % regarding WO_2. In the X–ray diffractogramm the only visible crystalline phases are WO_2 and W (see fig. 1).

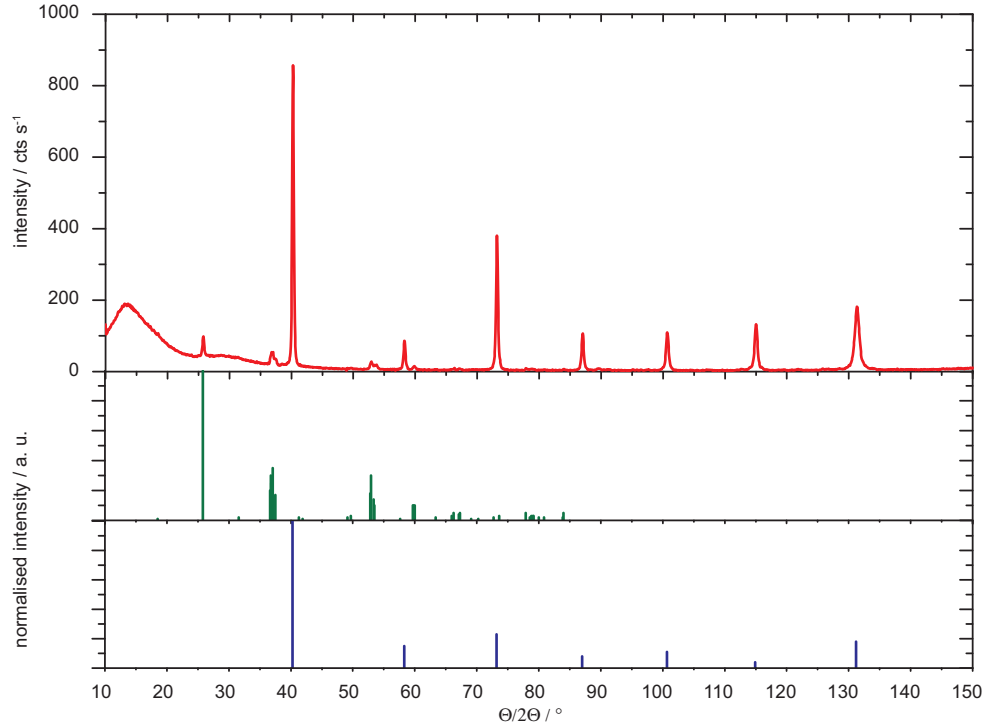

Figure 1. X–ray diffractogramm of the synthesised WO_2–substrate: The diffractogramm of the substrate (red) is compared to the reference data of the *PDF*–database of WO_2 (green) and W (blue).

The acquired XP–spectra are analyzed with the *MultiPak* software solution. [11] The binding energy scale was calibrated using gold, silver and copper samples and measuring the Au $4f_{7/2}$ core level at 84.0 eV, the Cu $2p_{3/2}$ core level at 932.7 eV, and the Ag $3d_{5/2}$ core level at 368.3 eV. [8,12,13] For peaks in the W 4*f*–spectra a Doniach–Šunjić–Function [14] is applied after subtracting a linear background. Peaks in the Be 1*s* and the O 1*s* binding energy region are analysed with a Gauss–Lorentz–Function and a Shirley–type background [15]. The pass energy of the analyser for the high resolution spectra is set to 2.95 eV and for the spectra of the valence band region to 29.35 eV, resulting in energy resolutions of

Preprints (www.preprints.org) | NOT PEER-REVIEWED | Posted: 2 July 2019 doi:10.20944/preprints201907.0028.v1

the hemispherical analyser of 0.04 eV respectively 0.44 eV. Taking the apparatus–function into account a maximum resolution of 0.1 eV is achievable for the high resolution spectra.

3. Data Analysis

In this section the approach used for data analysis to acquire informations about the chemical reactions will be evolved and explained in detail. First a chemical equation, which describes all reactions at the given temperature step, is derived out of the spectra. In the following these equation will be called main equation. In the final step the main equation is stripped down to the specific reaction equations.

Starting with the recorded spectra of the different core levels the involved compounds can already be determined. Every core level shows chemical shifts of the binding energy. These shifts depend on the chemical surrounding of the respective element. From these shifts the different compounds of the respective element can be identified. The spectra can the be deconvoluted and the amounts of the specific compounds are directly proportional to the integrals of the fit–functions. The signal contribution is heavily influenced by the depth distribution and so only signals originating from the same depth can be compared to gain quantitative information.

At the very beginning of the experiment the specimens consist of three layers. Beryllium and its oxide form the upper layer. The middle layer is made out of tungsten and its compounds, while the deepest layer is the tungsten substrate, which is out of the information depth of the experiment. For quantitative analysis the first two layers have to be considered. To avoid the influence of depth distribution only signals originating from one of these layers are usable. For this reason, the O 1*s* spectral region is not suitable, because it delivers information from both the beryllium oxide in the upper layer as well as from the the different tungsten oxygen compounds in the middle layer. The same is true for the Be 1*s* binding energy region.

The spectra of the W 4*f*–core levels reveals only informations about the middle layer. Additionally, tungsten is very mobile, thus a homogeneous distribution of its compounds in this layer can be assumed. [16] So, the W 4*f*–spectra is perfectly suited for the requirements for quantitative analysis.

With this assumption the intensity of the W 4*f*–spectra only changes with the amount of the compounds and the thickness of the beryllium layer above the tungsten oxide layer. In order to eliminate the influence of the thickness of the beryllium layer only the relative composition of the complete signal is taken into account and not the absolute values. Since only signals from the same core level and the same element are used, even the element specific cross sections can be neglected.

In addition, the diffusion of beryllium and its oxide does not influence data analysis as long as one can assume, that the beryllium compounds are distributed homogeneously throughout the beryllium layer. Even the tungsten oxide layer only gets diluted by a homogeneous contamination of beryllium compounds resulting in a weaker intensity of the signal but not in a change of the fractions of the specific signal contributions.

The spectra of the Be 1*s* and the O 1*s* binding energy region provide valuable qualitative information, which is used to verify the results of the analysis of the tungsten spectra.

For the rates of chemical reactions at a given temperature only the change of the concentrations of the compounds is important. Therefore, the difference of the signal contribution of the current and the preceding temperature step is calculated. The results are used as stoichiometric factors in the main equation. Negative values mean a decrease of the specific compounds, positive values an increase of the specific compound. With the informations from the qualitative analysis of the beryllium spectra the element balance can be agreed. With this step, the main reaction equation is complete.

In the next step the main reaction equation I is decomposed in the individual reaction equations II, III,.... Therefore, all chemical sensible equations are set up in a system of equations. The result is the main equation:

$$\mathrm{I} = a \cdot \mathrm{II} + b \cdot \mathrm{III} + ... \tag{1}$$

Preprints (www.preprints.org) | NOT PEER-REVIEWED | Posted: 2 July 2019 doi:10.20944/preprints201907.0028.v1

When solving these system, prefactors $a, b, ...$ for each chemical reaction are obtained. These prefactors are a measure for the reaction rate at the specific temperature. The ratios of the prefactors are the same as the ratios of the rate constants.

The experimental procedure and the subsequent data analysis can be summarised as follows:

1. Heating the sample to the desired temperature
2. Recording high resolution spectra of the Be 1*s*, O 1*s*, and W 4*f* and valence band spectra
3. Spectral deconvolution of the spectra to identify and quantify elements and compounds
4. Compare the results to the previous temperature step and set up the main chemical equation
5. Identify possible chemical reactions
6. Solve the linear equation system to obtain the prefactors for the single reaction equations

4. Results

Both oxidic tungsten specimens are coated with a thin beryllium layer by physical vapour deposition. Each sample is heated in 100 K–steps from 573 K to 1273 K. Each heating step takes 30 min. After each heating step, the sample is cooled down and the spectra are taken with sample temperatures below 373 K. Below the binding energies of the W $4f_{7/2}$–peak are given. The corresponding W $4f_{5/2}$–peak is at 2.18 eV higher binding energies.

4.1. Be on WO_3

4.1.1. Analysis of the spectra

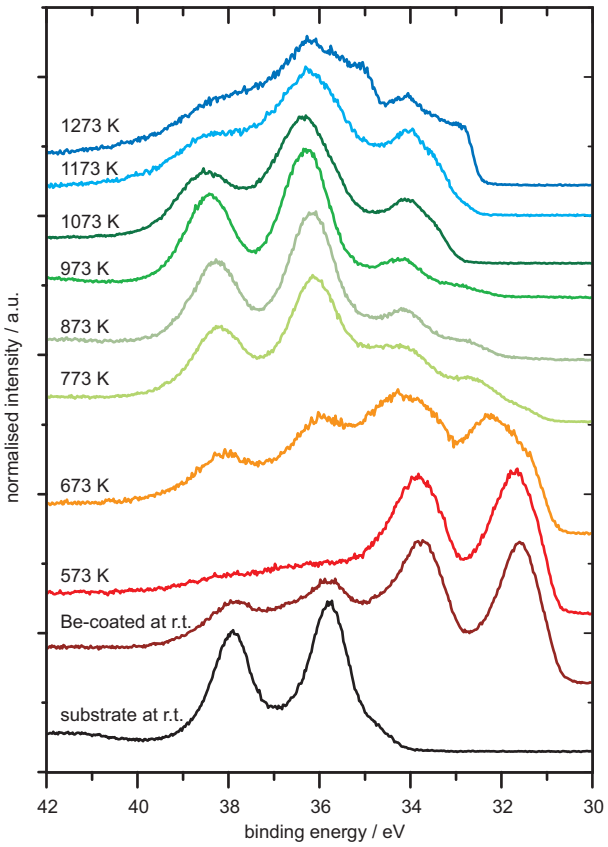

Figure 2. W 4*f*–spectra of the coated tungsten trioxide specimen

In this section the analysis of the spectra of the evaporated tungsten trioxide sample is described. The core level spectra of the W 4*f*–region are shown in figure 2, the Be 1*s*–spectra in figure 3, and the

Preprints (www.preprints.org) | NOT PEER-REVIEWED | Posted: 2 July 2019 doi:10.20944/preprints201907.0028.v1

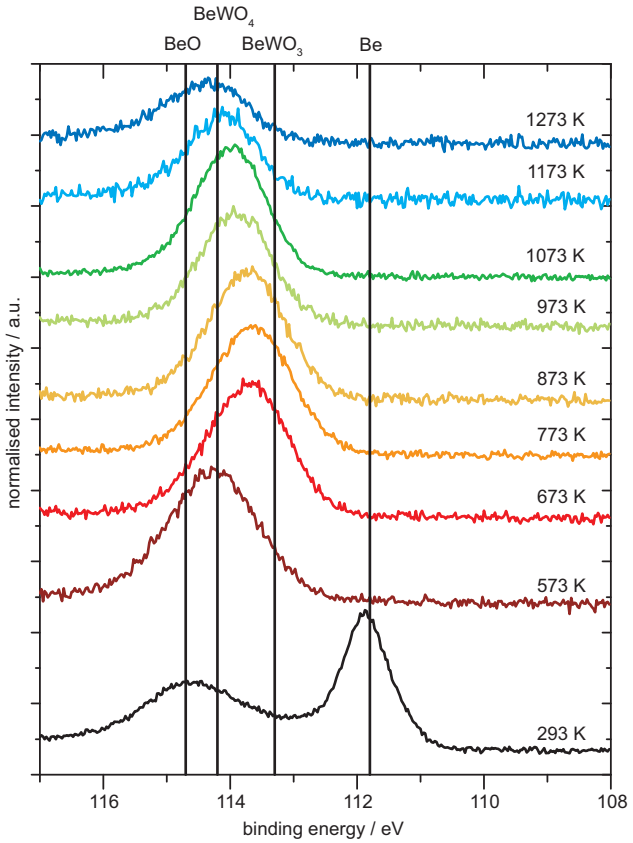

Figure 3. Be 1*s*–spectra of the coated tungsten trioxide specimen

valence band spectra in figure 4. The results of the spectral deconvolution are discussed in detail. All results of the deconvolution of the W 4*f* spectra are compiled in table 1. A graphical representation of the sample composition at each temperature step is shown in figure 5. In the following the spectra analysis is described in detail.

In the W 4*f*–spectrum (see fig. 2) of the Be–coated WO_3–sample six different compounds can be identified at r. t. The peaks at 32.9 eV, 34.5 eV and 35.7 eV originate from the three oxidic species WO_2, WO_{3-x} and WO_3. [17–25] At a binding energy of 31.3 eV the peak of elemental tungsten is visible. The two remaining peaks at 31.7 eV and 35.7 eV originate from the tungsten bronze $BeWO_3$ and from the beryllium tungstate $BeWO_4$. [26,27] The tungsten oxides are immediately reduced by the evaporated beryllium and the tungstate and the tungsten bronze are also formed. In the Be 1*s*–spectrum (s. fig. **??**) four peaks can be identified. The two peaks with the highest intensity at 118.8 eV and 114.7 eV originate from elemental beryllium and its oxide BeO. [21,28–33] The two smaller peaks at 114.2 eV and 113.3 eV originate from the tungstate respectively from the bronze. The ratios of the signal intensities of these two compounds in the W 4*f*– and the Be 1*s*–spectra match. A new peak forms in the spectrum of the valence shell (s. fig. 4) at 2.6 eV, which is assigned to the beryllium compounds. The broad peak at 7.2 eV belonging to WO_3 slightly looses intensity as WO_3 is consumed.

At 573 K the oxidation of beryllium is finished as you cannot see elemental Be in the spectrum anymore. The signal contributions of WO_3, WO_{3-x} and tungsten decrease. Out of these three compounds the tungstates and tungsten dioxide are formed. The signal contribution of $BeWO_3$ reaches its maximum, while the contributions of WO_3 and WO_{3-x} reach their minimum. Nearly half of the signal originates from the tungsten bronze. In the valence shell spectrum the peak at 7.2 eV gets more shallow.

In the next temperature step at 673 K, the signal of metallic tungsten decreases even more. The signal contributions of the oxidic tungsten compounds increase. The signal contribution of the

Preprints (www.preprints.org) | NOT PEER-REVIEWED | Posted: 2 July 2019 doi:10.20944/preprints201907.0028.v1

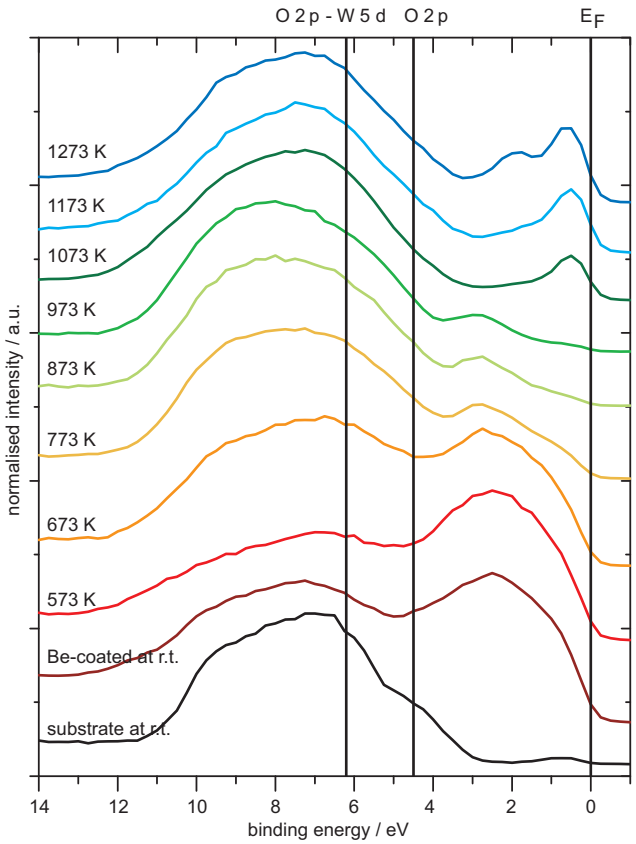

Figure 4. Valence band spectra of the coated tungsten trioxide specimen

beryllium tungstate decreases, while the contribution of the bronze increases. The peak at 2.2 eV shifts to higher binding energies at 2.8 eV.

At 773 K the signal contributions of the compounds WO_2 and $BeWO_3$ decrease, while all other contributions increase.

The contributions of metallic tungsten and $BeWO_3$ vanish at a temperature of 873 K. The signal of WO_3 reaches its maximum. The other peak areas nearly stay the same.

At 973 K all oxidic tungsten compounds decrease while the signal contribution of $BeWO_4$ nearly doubles from 24.9 % to 46.5 % and reaches its maximum.

At 1073 K, the substoichiometric oxides increase their fraction from 21.5 % to 41.6 %, while WO_3 reaches its local minimum of 18.5 %. The signal contribution of the tungstate drops by 6.6 %. In the spectrum of the valence shell a new peak evolves at 0.4 eV. This peak is assigned to the W 5*d*–Orbitals of tungsten. [17] In the spectrum of the pure substrate this peak has a much lower intensity. A small part of the increase is caused by the higher order of the tungsten trioxide and the substoichiometric oxide. But most of the gain is assigned to the tungstate.

Tungsten dioxide completely vanishes at a temperature of 1173 K. The decomposition of $BeWO_4$ proceeds. Accordingly the contributions of the oxides WO_3 and WO_{3-x} increase.

In the final temperature step at 1273 K the contribution of $BeWO_4$ further shrinks. WO_2 again is formed and has a share of the overall signal of 7.3 %. Here, WO_2 is only a decay intermediate, since at 1273 K it is not stable. The substoichiometric oxides slighly decreas while the contribution of WO_3 slightly increases. In the spectrum of the valence shell a new peak evolves at 2.8 eV, which is assigned

Preprints (www.preprints.org) | NOT PEER-REVIEWED | Posted: 2 July 2019 doi:10.20944/preprints201907.0028.v1

Table 1. Signal contributions for the evaporated tungsten trioxide specimen at the different temperature T steps

	Signal contributions of the W 4*f*–region [%]					
T [K]	W	WO_2	WO_{3-x}	WO_3	$BeWO_3$	$BeWO_4$
293	13.0	7.8	14.8	19.6	37.2	7.6
573	11.6	13.2	10.5	7.5	47.2	10.0
673	9.4	14.7	15.3	15.0	30.6	15.1
773	2.6	9.4	22.3	30.8	11.9	22.9
873	0.0	9.8	23.4	45.3	0.0	21.6
973	0.0	4.7	20.2	28.6	0.0	46.5
1073	0.0	0.3	41.6	18.3	0.0	39.9
1173	0.0	0.0	43.3	34.3	0.0	22.4
1273	0.0	7.3	40.8	35.2	0.0	16.7

to WO_2.

4.1.2. Quantitative Analysis

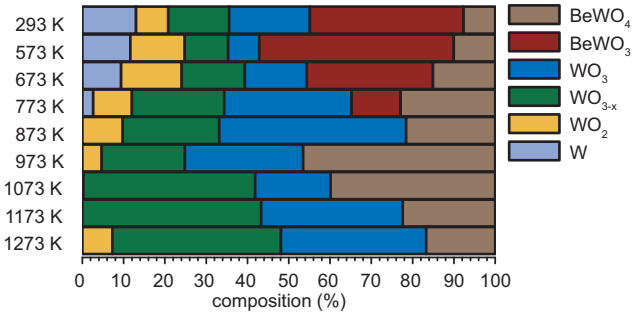

Figure 5. Composition of the Be-coated tungsten trioxide specimen

In this part, the reactions at each temperature step will be given. For the first temperature step the analysis is given in detail as a practical example of the application of the model, while for the following steps only the results are given. Since WO_3 and WO_{3-x} are chemically nearly identical, their signal contributions are united in the following section.

573 K

At first, the signal contributions from the preceding heating step, here 273 K, have to be substracted from the signal contributions of the current heating step. As stated above (s. sec. 3) these values give the alteration of the concentrations of each compound. The result can be written as:

$$\underbrace{1.4\mathrm{W} + 16.3\mathrm{WO_3}}_{17.7\mathrm{W,48.9O}} \approx \underbrace{5.4\mathrm{WO_2} + 9.9\mathrm{BeWO_3} + 2.4\mathrm{BeWO_4}}_{17.7\mathrm{W,50.1O,12.3Be}} \tag{2}$$

Next, the elemental balances have to be agreed. For this, it is only allowed to consider compounds without tungsten, since eq. 2 is already based on the W 4*f*–signal. In the Be 1*s*–spectrum Be and BeO can be seen additional to the tungstate and the bronze (s. fig. **??**). These compounds are used to agree the balance and we get:

$$\text{I:} \quad \underbrace{1.4\mathrm{W} + 16.3\mathrm{WO_3} + 1.2\mathrm{BeO} + 11.1\mathrm{Be}}_{17.7\mathrm{W,50.1O,12.3Be}} \longrightarrow \underbrace{5.4\mathrm{WO_2} + 9.9\mathrm{BeWO_3} + 2.4\mathrm{BeWO_4}}_{17.7\mathrm{W,50.1O,12.3Be}} \tag{3}$$

Preprints (www.preprints.org) | NOT PEER-REVIEWED | Posted: 2 July 2019 doi:10.20944/preprints201907.0028.v1

Now the reactions for the system of equation are set up:

$$\begin{aligned}
\text{II:} \quad & 2WO_2 + W \longrightarrow 3WO_3 && (4)\\
\text{III:} \quad & WO_3 + Be \longrightarrow WO_2 + BeO && (5)\\
\text{IV:} \quad & WO_3 + BeO \longrightarrow BeWO_4 && (6)\\
\text{V:} \quad & WO_2 + BeO \longrightarrow BeWO_3 && (7)\\
\text{VI:} \quad & WO_3 + Be \longrightarrow BeWO_3 && (8)
\end{aligned}$$

As shown in eq. 1 the overall equation is now decomposed:

$$\text{I} = a \cdot \text{II} + b \cdot \text{III} + c \cdot \text{IV} + d \cdot \text{V} + e \cdot \text{VI} \tag{9}$$

After solving eq. 9 the following prefactors are achieved:

$$a = 1.4 \quad b = 1.2 \quad c = 2.4 \quad d = 0.0 \quad e = 9.9$$

The obtained prefactors comply with the weighting of each single reaction at the current heating step. While reaction V does not take place, the formation of beryllium tungsten bronze is by far the most important reaction at this temperature.

673 K

For the following temperature steps only the complete chemical equation, the individual chemical equations and the solution of the system of equations are given.

$$\text{I:} \quad 2.2W + 16.6BeWO_3 + 10.9O_2 \longrightarrow 1.5WO_2 + 12.3WO_3 + 5.0BeWO_4 + 11.6BeO \tag{10}$$

Here, the main equation also could be agreed by using metallic beryllium and beryllium oxide. But since there is no beryllium in the Be 1*s*–spectrum, this possibility is excluded. Additionally, beryllium oxide is stable at this temperature. Nonetheless the oxygen content of the specimen rises. for this reasons oxygen and beryllium oxide are used to agree the main equation. The reactions taking place are:

$$\begin{aligned}
\text{II:} \quad & WO_3 + BeO \longrightarrow BeWO_4 && (11)\\
\text{III:} \quad & W + \tfrac{3}{2}O_2 \longrightarrow WO_3 && (12)\\
\text{IV:} \quad & W + 2\,WO_3 \longrightarrow WO_2 && (13)\\
\text{V:} \quad & BeWO_3 + \tfrac{1}{2}O_2 \longrightarrow BeO + WO_3 && (14)
\end{aligned}$$

$$\text{I} = 5 \cdot \text{II} + 1.7 \cdot \text{III} + 0.5 \cdot \text{IV} + 16.6 \cdot \text{V} \tag{15}$$

773 K

$$\text{I:} \quad 6.8W + 5.3WO_2 + 18.7BeWO_3 + 22.2O_2 \longrightarrow 22.9WO_3 + 7.9BeWO_4 + 10.8BeO \tag{16}$$

At this temperature the oxygen amount still increases. The reactions at these step are:

Preprints (www.preprints.org) | NOT PEER-REVIEWED | Posted: 2 July 2019 doi:10.20944/preprints201907.0028.v1

$$\begin{aligned} \text{II:} \quad & WO_3 + BeO \longrightarrow BeWO_4 && (17)\\ \text{III:} \quad & W + \tfrac{3}{2}O_2 \longrightarrow WO_3 && (18)\\ \text{IV:} \quad & WO_2 + \tfrac{1}{2}O_2 \longrightarrow WO_3 && (19)\\ \text{V:} \quad & BeWO_3 + \tfrac{1}{2}O_2 \longrightarrow BeO + WO_3 && (20) \end{aligned}$$

$$I = 7.9 \cdot II + 6.8 \cdot III + 5.3 \cdot IV + 18.7 \cdot V \quad (21)$$

873 K

$$\text{I:} \quad 2.6W + 11.9BeWO_3 + 1.4BeWO_4 + 9.7O_2 \longrightarrow 0.37WO_2 + 15.47WO_3 + 13.3Beo \quad (22)$$

Here, the amount of oxygen increases further. For this reason the main reaction is still agreed with BeO and O_2. The following reactions take place:

$$\begin{aligned} \text{II:} \quad & BeWO_4 \longrightarrow BeO + WO_3 && (23)\\ \text{III:} \quad & BeWO_3 + \tfrac{1}{2}O_2 \longrightarrow BeO + WO_3 && (24)\\ \text{IV:} \quad & W + 2WO_3 \longrightarrow 3\,WO_2 && (25)\\ \text{V:} \quad & W + \tfrac{3}{2}O_2 \longrightarrow WO_3 && (26) \end{aligned}$$

$$I = 1.4 \cdot II + 11.9 \cdot III + 0.13 \cdot IV + 2.5 \cdot V \quad (27)$$

973 K

$$\text{I:} \quad 5.1WO_2 + 19.8WO_3 + 24.9BeO + 2.6O_2 \longrightarrow 24.9BeWO_4 \quad (28)$$

The amount of oxygen keeps increasing and the following reactions take place:

$$\begin{aligned} \text{II:} \quad & WO_2 + \tfrac{1}{2}O_2 \longrightarrow WO_3 && (29)\\ \text{III:} \quad & BeO + WO_3 \longrightarrow BeWO_4 && (30) \end{aligned}$$

$$I = 5.1 \cdot II + 24.9 \cdot III \quad (31)$$

1073 K

At this step the model does not deliver sensible informations. This means in reverse that one of the made assumptions cannot be applied here. Most likely, the specimen is under the diffusion regime, so the model cannot be used here.

1173 K

$$\text{I:} \quad 0.2WO_2 + 17.5BeWO_4 + 0.1O_2 \longrightarrow 17.7WO_3 + 17.5BeO \quad (32)$$

Preprints (www.preprints.org) | NOT PEER-REVIEWED | Posted: 2 July 2019 doi:10.20944/preprints201907.0028.v1

At these temperature the decomposition of $BeWO_4$ to BeO and WO_3 is the main reaction. Reaction III is a diffusion artifact, since the reaction does not take place at this temperature. The prefactor for this reaction is only 0.2. Thus, the error is negligible.

$$\text{II:} \quad BeWO_4 \longrightarrow WO_3 + BeO \tag{33}$$
$$\text{III:} \quad WO_2 + \tfrac{1}{2}O_2 \longrightarrow WO_3 \tag{34}$$
$$\tag{35}$$

$$\text{I} = 17.5 \cdot \text{II} + 0.2 \cdot \text{III} \tag{36}$$

1273 K

$$\text{I:} \quad 5.7BeWO_4 + 1.6WO_3 \longrightarrow 7.3WO_2 + 5.7BeO + 3.6O_2 \tag{37}$$

The decomposition of $BeWO_4$ continues. The created tungsten trioxide decomposes immediately to WO_2 and O_2. Here, the rate determing step is the decomposition reaction of $BeWO_4$.

$$\text{II:} \quad BeWO_4 \longrightarrow WO_3 + BeO \tag{38}$$
$$\text{III:} \quad WO_3 \longrightarrow WO_2 + \frac{1}{2}O_2 \tag{39}$$

$$\text{I} = 5.7 \cdot \text{II} + 7.3 \cdot \text{III} \tag{40}$$

4.2. Be on WO_2

4.2.1. Analysis of the spectra

In this section the analysis of the spectra of the tungsten dioxide based sample is described. The core level spectra of the W 4*f*–region are shown in figure 6, the Be 1*s*–spectra in figure 7, and the valence band spectra in figure 8. All results of the deconvolution of the W 4*f*–spectra of the WO_2–sample are compiled in table 2. A graphical representation of the sample composition at each temperature step is shown in figure 9. In the following the spectra analysis is described in detail.

After coating the substrate six compounds can be identified. The peak pairs of the oxidic tungsten compounds are at 32.9 eV (WO_2), 34.7 eV (WO_{3-x}) and 35.8 eV (WO_3). The metallic tungsten causes the peak at 31.4 eV. The beryllium tungsten bronze has a binding energy of 31.7 eV, and the tungstate of 36.6 eV (s. fig. 6). The tungsten dioxide is not reduced by the metallic beryllium. In the Be 1*s*–spectrum four compounds can be identified: Beryllium at 111.8 eV, $BeWO_3$ at 113.4 eV, $BeWO_4$ at 114.2 eV and beryllium oxide at 114.7 eV (s. fig. 7). The peak relation of the bronze and the tungstate in the W 4*f*– and the Be 1*s*–spectrum are the same. In the valence shell region the intensity of the broad peak between 6.8 eV and 9.2 eV decreases. The clearly defined peak at 0.8 eV assigned to WO_2 looses intensity und becomes a shoulder of the peak at 2.1 eV (s. fig. 8).

The oxidation of beryllium is finished at a temperature of 573 K. The signal contribution of the bronze increases and reaches its maximum. Accordingly, the peak in the Be 1*s*–spectrum shifts to lower binding energies. The signal contributions of all other compounds in the W 4*f*–spectrum decrease.

In the next temperature step the contribution of WO_2 increases by 9.8 %. The contributions of WO_3 and $BeWO_4$ also increase. The peaks of all other species decrease.

At 773 K the contributions do not change significantly.

In the next step, only the signal of elementary tungsten shows a decline. There is no change in the Be 1*s* and the valence shell spectrum.

Preprints (www.preprints.org) | NOT PEER-REVIEWED | Posted: 2 July 2019 doi:10.20944/preprints201907.0028.v1

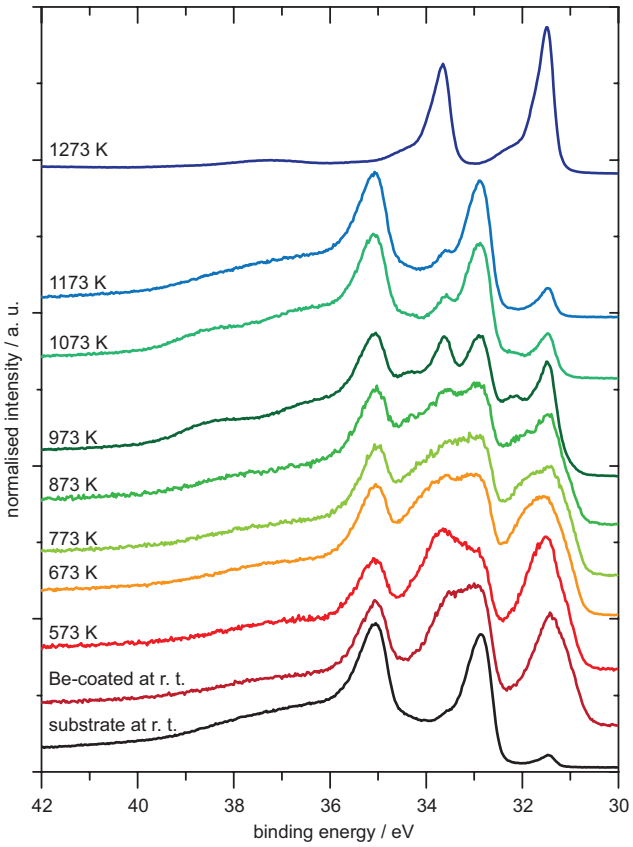

Figure 6. W 4*f*–spectra of the coated tungsten dioxide specimen

At 973 K, the signal contribution of $BeWO_4$ increases while the signal of $BeWO_3$ decreases. The signal of metallic tungsten still decreases. The peaks of the oxidic compounds WO_2 and WO_3 rise. The contribution of the substoichiometric oxides stay constant. In the other spectra no change is to be seen.

The signal contribution of the tungstate reaches its maximum at 1073 K. The share of the signal contribution of the bronze decreases by 9.7 %, and the share of the metallic tungsten by 8.7 %. The signal contribution of WO_3 decreases while the contributions of the other compounds increase. The shoulder in the valence shell spectrum at 0.8 eV becomes a discrete peak.

In the last temperature step the complete WO_2 and the beryllium tungsten compounds are decomposed. The metallic tungsten makes 85.3 % of the W 4*f*–peak. The rest of the signal originates from WO_3 and WO_{3-x}. In the Be 1*s*–spectrum, there are also no beryllium tungsten compounds. The signal of the Be 1*s*–region consists by 49.8 % of beryllium oxide. The rest of the Be 1*s*–signal is also assigned to beryllium oxide since there are no beryllium tungstate species anymore and no other compounds containing beryllium can be found in this sample.

4.2.2. Quantitative Analysis

In the following the model described in sec. 3 is used. For the examples see eq. 2–9.

573 K

$$\text{I:}\quad 5.8W + 4.6WO_2 + 0.5WO_3 + 1.0BeWO_4 + 11.9Be + 11.0O_2 \longrightarrow 11.9BeWO_3 + 1.0BeO \qquad (41)$$

Preprints (www.preprints.org) | NOT PEER-REVIEWED | Posted: 2 July 2019 doi:10.20944/preprints201907.0028.v1

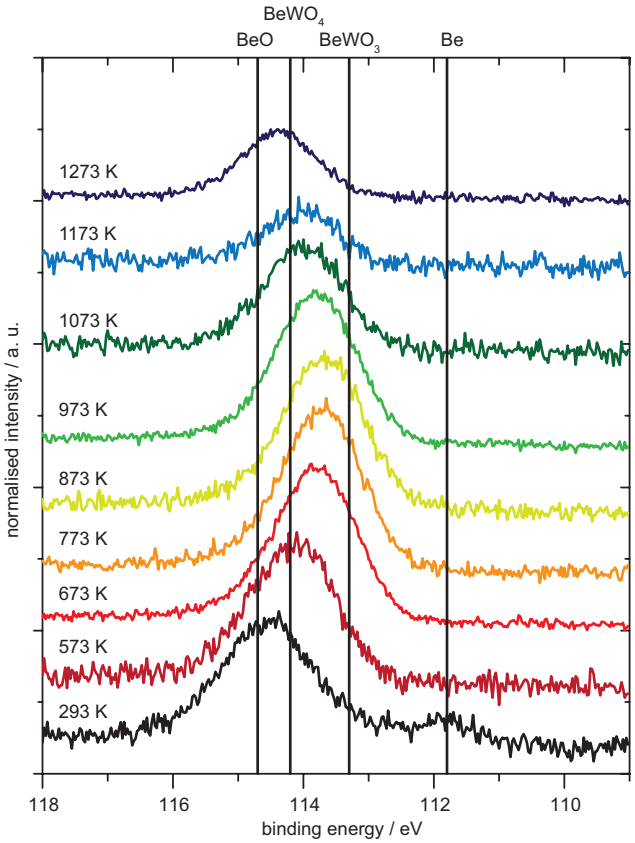

Figure 7. Be 1*s*–spectra of the coated tungsten dioxide specimen

$$\text{II:} \quad WO_2 + \tfrac{1}{2}O_2 \longrightarrow WO_3 \tag{42}$$
$$\text{III:} \quad W + \tfrac{3}{2}O_2 \longrightarrow WO_3 \tag{43}$$
$$\text{IV:} \quad WO_3 + BeO \longrightarrow BeWO_4 \tag{44}$$
$$\text{V:} \quad BeWO_4 + Be \longrightarrow BeWO_3 \tag{45}$$

$$I = 4.6 \cdot II + 5.8 \cdot III + 10.9 \cdot IV + 11.9 \cdot V \tag{46}$$

At this temperature step only the reductive synthesis of the tungsten bronze takes place.

673 K

$$1.8W + 2.8WO_3 + 5.9BeWO_3 + 0.8O_2 \longrightarrow 9.7WO_2 + 0.8BeWO_4 + 5.1BeO \tag{47}$$

$$\text{II:} \quad WO_3 + BeO \longrightarrow BeWO_4 \tag{48}$$
$$\text{III:} \quad W + O_2 \longrightarrow WO_2 \tag{49}$$
$$\text{IV:} \quad W + 2WO_3 \longrightarrow 3WO_2 \tag{50}$$
$$\text{V:} \quad BeWO_3 \longrightarrow BeO + WO_2 \tag{51}$$

Preprints (www.preprints.org) | NOT PEER-REVIEWED | Posted: 2 July 2019 doi:10.20944/preprints201907.0028.v1

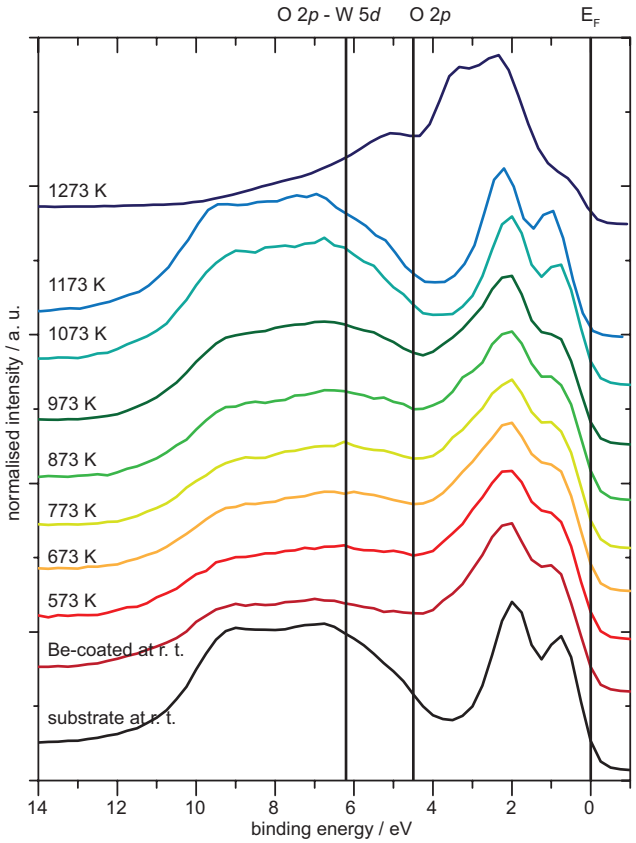

Figure 8. Valence band spectra of the coated tungsten dioxide specimen

$$\mathrm{I} = 0.8 \cdot \mathrm{II} + 0.8 \cdot \mathrm{III} + 1.0 \cdot \mathrm{IV} + 5.9 \cdot \mathrm{V} \tag{52}$$

Remarkably the tungsten bronze dissociates via a different reaction.

773 K

$$\mathrm{I:}\quad 1.8\mathrm{BeWO_3} \longrightarrow 0.5\mathrm{W} + 0.3\mathrm{WO_2} + 0.5\mathrm{WO_3} + 0.5\mathrm{BeWO_4} \tag{53}$$

The tungsten bronze dissociates to WO_2 and BeO. W and WO_3 is formed by disproportioning. BeO and WO_3 form the tungstate.

$$\mathrm{II:}\quad \mathrm{BeWO_3} \longrightarrow \mathrm{WO_2} + \mathrm{BeO} \tag{54}$$

$$\mathrm{III:}\quad 3\mathrm{WO_2} \longrightarrow 2\mathrm{WO_3} + \mathrm{W} \tag{55}$$

$$\mathrm{IV:}\quad \mathrm{WO_3} + \mathrm{BeO} \longrightarrow \mathrm{BeWO_4} \tag{56}$$

$$\mathrm{I} = 1.8 \cdot \mathrm{II} + 0.5 \cdot \mathrm{III} + 0.5 \cdot \mathrm{IV} \tag{57}$$

873 K

$$\mathrm{I:}\quad 3.7\mathrm{W} + 1.4\mathrm{BeO} + 4.1\mathrm{O_2} \longrightarrow 1.5\mathrm{WO_2} + 0.8\mathrm{WO_3} + 1.4\mathrm{BeWO_3} \tag{58}$$

Preprints (www.preprints.org) | NOT PEER-REVIEWED | Posted: 2 July 2019 doi:10.20944/preprints201907.0028.v1

Table 2. Signal contributions for the evaporated tungsten dioxide specimen at the different temperature steps

	Signal contributions of the W 4*f*–region [%]					
Temperature [K]	W	WO_2	WO_{3-x}	WO_3	$BeWO_3$	$BeWO_4$
293	28.5	25.6	20.8	4.5	16.0	4.7
573	22.7	21.0	20.1	4.8	27.8	3.7
673	21.0	30.7	16.2	5.7	21.9	4.5
773	21.5	31.0	17.2	5.2	20.1	5.0
873	17.8	32.5	16.0	7.2	21.5	5.0
973	18.5	33.8	15.5	8.3	15.1	8.8
1073	9.8	36.7	29.9	6.9	5.8	10.9
1173	5.8	44.4	31.4	8.2	2.4	7.8
1273	85.3	0.0	4.0	9.7	0.0	0.0

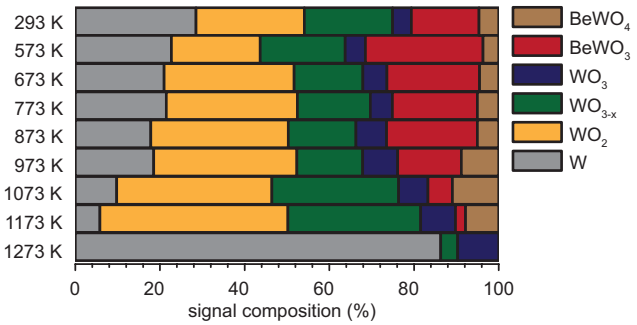

Figure 9. Composition of the Be-coated tungsten dioxide specimen

At these temperature step the tungsten bronze is synthesised via the tungstate as seen above. As there is no metallic Beryllium to be seen in the Be 1*s*–spectrum, tungsten instead of beryllium acts as reduction agent here.

$$\text{II:} \quad W + \tfrac{3}{2}O_2 \longrightarrow WO_3 \tag{59}$$

$$\text{III:} \quad BeO + WO_3 \longrightarrow BeWO_4 \tag{60}$$

$$\text{IV:} \quad 3BeWO_4 + W \longrightarrow 3BeWO_3 + WO_3 \tag{61}$$

$$\text{V:} \quad W + O_2 \longrightarrow WO_2 \tag{62}$$

$$\text{I} = 1.7 \cdot \text{II} + 1.4 \cdot \text{III} + 0.5 \cdot \text{IV} + 1.5 \cdot \text{V} \tag{63}$$

At these step there are two reactions; the formation of tungsten bronze and the oxidation of tungsten to tungsten dioxide.

973 K

$$\text{I:} \quad 6.4BeWO_3 + 1.5O_2 \longrightarrow 3.8BeWO_4 + 1.3WO_2 + 0.7W + 0.6WO_3 + 2.6BeO \tag{64}$$

At this step, the tungsten bronze essentially decays or is converted to tungstate.

Preprints (www.preprints.org) | NOT PEER-REVIEWED | Posted: 2 July 2019 doi:10.20944/preprints201907.0028.v1

$$\text{II:} \quad BeWO_3 + \tfrac{1}{2}O_2 \longrightarrow BeWO_4 \tag{65}$$
$$\text{III:} \quad BeWO_3 \longrightarrow BeO + WO_2 \tag{66}$$
$$\text{IV:} \quad BeO + WO_3 \longrightarrow BeWO_4 \tag{67}$$
$$\text{V:} \quad 3WO_2 \longrightarrow 2WO_3 + W \tag{68}$$

$$\text{I} = 3.0 \cdot \text{II} + 3.4 \cdot \text{III} + 0.8 \cdot \text{IV} + 0.7 \cdot \text{V} \tag{69}$$

1073 K

$$\text{I:} \quad 8.8W + 9.3BeWO_3 + 16.4O_2 \longrightarrow 2.9WO_2 + 13.1WO_3 + 2.1BeWO_4 + 6.8BeO \tag{70}$$

At this temperature step mainly tungsten trioxide and beryllium tungstate are formed.

$$\text{II:} \quad BeWO_3 + \tfrac{1}{2}O_2 \longrightarrow BeWO_4 \tag{71}$$
$$\text{III:} \quad BeWO_4 \longrightarrow BeO + WO_3 \tag{72}$$
$$\text{IV:} \quad W + O_2 \longrightarrow WO_2 \tag{73}$$
$$\text{V:} \quad BeWO_3 \longrightarrow BeO + WO_2 \tag{74}$$
$$\text{VI:} \quad W + \tfrac{3}{2}O_2 \longrightarrow WO_3 \tag{75}$$

$$\text{I} = 8.9 \cdot \text{II} + 6.8 \cdot \text{III} + 2.5 \cdot \text{IV} + 0.4 \cdot \text{V} + 6.3 \cdot \text{VI} \tag{76}$$

1173 K

$$\text{I:} \quad 3.9W + 3.4BeWO_3 + 3.1BeWO_4 + 3.7O_2 \longrightarrow 7.7WO_2 + 2.7WO_3 + 6.5BeO \tag{77}$$

At this temperature step we see a huge increase of tungsten dioxide.

$$\text{II:} \quad BeWO_3 \longrightarrow WO_2 + BeO \tag{78}$$
$$\text{III:} \quad BeWO_4 \longrightarrow WO_3 + BeO \tag{79}$$
$$\text{IV:} \quad W + 2WO_3 \longrightarrow 3WO_2 \tag{80}$$
$$\text{V:} \quad W + O_2 \longrightarrow WO_2 \tag{81}$$

$$\text{I} = 3.4 \cdot \text{II} + 3.1 \cdot \text{III} + 0.2 \cdot \text{IV} + 3.7 \cdot \text{V} \tag{82}$$

1273 K

At the last temperature step, we see a reduction of tungsten dioxide and tungsten trioxide.

$$\text{I:} \quad 44.4WO_2 + 25.9WO_3 + 7.8BeWO_4 + 2.4BeWO_3 \longrightarrow 80.5W + 10.2BeO + 97.3O_2 \tag{83}$$

Preprints (www.preprints.org) | NOT PEER-REVIEWED | Posted: 2 July 2019 doi:10.20944/preprints201907.0028.v1

$$\text{II:} \quad BeWO_3 \longrightarrow WO_2 + BeO \tag{84}$$

$$\text{III:} \quad BeWO_4 \longrightarrow WO_3 + BeO \tag{85}$$

$$\text{IV:} \quad WO_3 \longrightarrow W + \tfrac{3}{2}O_2 \tag{86}$$

$$\text{V:} \quad WO_2 \longrightarrow W + O_2 \tag{87}$$

$$I = 2.4 \cdot II + 7.8 \cdot III + 25.9 \cdot IV + 44.4 \cdot V \tag{88}$$

5. Discussion

5.1. The System Beryllium–Oxygen–Tungsten

In the preceding sections the reactions of the two investigated ternary systems are determined. To enable these reactions, beryllium and beryllium oxide have to diffuse into the tungsten oxide layer.

Tungsten trioxide and the substoichiometric tungsten oxide show a high diffusivity due to their structure. In these two compounds, tungsten atoms are coordinated octahedrally by oxygen atoms. These coordination octahedrons are linked by their corners. This structure shows channels in all three spatial directions through the whole crystal. This structure makes the diffusion possible.

Another point is the structure of tungsten bronze. In this compound the beryllium ions are embedded in these channels. So, the size of the channels is big enough for the beryllium ions.

On the contrary, tungsten dioxide is surprisingly inert. It shows no reaction until it dissociates at 1273 K. Tungsten dioxide has rutile structure. The rutile structure does not form any channels, so no diffusion into the bulk is possible. Therefore, reactions can only take place at the surface of the crystallites and are negligibly slow.

Nevertheless, in the survey spectra, diffusion can be seen. The diffusion can take place along the grain boundaries.

In the binary system beryllium–tungsten, the formation of alloys takes place. [8,28,29] Here, alloy formation can not be observed in the ternary system Be–O–W. So, the ternary system show a completely different chemistry.

5.2. The Model

As mentioned above (s. sec. 3), a homogeneous distribution of the chemically different species is assumed. The model cannot cope with diffusive processes. For the Be–coated tungsten trioxide specimen, an approximately homogeneous distribution can be assumed due to the high mobility of the Be–ions in a WO_3–lattice. Additionally, the various chemical reaction in this specimen do their share for a homogenous mixing. Finally, the model delivers results for each temperature step, which are consistent with the observed spectra. For these reasons, the assumption of a homogeneous distribution in the oxide layer is permissible.

Even for the tungsten dioxide layer a homogeneous distribution can be assumed. At the beginning, the oxide layer of this sample can be divided into two parts; on the one hand there is the product WO_2, on the other hand the byproduct WO_3. For the byproduct the same is true as for the tungsten trioxide layer. However, the WO_2 is nearly inert and does not participate in any chemical reaction until it finally dissociates at a temperature of 1273 K. It can be assumed, that the distribution of WO_2 at the beginning is homogeneous. Since there is actually no change in the tungsten dioxide the distribution can be considered as static throughout the experiment until it dissociates.

The results achieved by this model are all chemically sensible, so this is also an evidence for its validity.

One of the model's weaknesses is there is no proof of the uniquiness of the obtained solution. However, the number of results can be decreased significantly by using the informations from the Be 1*s*–spectra and the survey–spectra.

In conclusion the model is well suited to gain chemical informations from the XP–spectra and is a valuable tool for the investigation of highly complex systems.

Funding: This research received no external funding.

Acknowledgments: All experiments are conducted at the Max–Planck–Institut für Plasmaphysik, Boltzmannstr. 2, 85748 Garching, Germany. This study is an excerpt of the master thesis "Investigation of the Ternary System Tungsten–Oxygen–Beryllium" [34] by Martin Köppen at the Technical University of Munich, Department of Chemistry, 85748 Garching, Germany. The author gratefully thanks Michael Fußeder and Florian Kost for the introduction to the XPS experimental setup and for their help in laboratory, Christian Linsmeier for hosting me in his group, Ulrich Heiz for academic supervision, Stefan Elgeti for his help with the XRD measurements and special thanks to Maren Hellwig for proof–reading.

Conflicts of Interest: The author declares no conflict of interest.

Abbreviations

The following abbreviations are used in this manuscript:

r. t.	room temperature
XPS	x–ray photoelectron spectroscopy
XRD	x–ray diffraction

References

1. Patel, K.J.; Desai, M.S.; Panchal, C.J.; Deota, H.N.; Trivedi, U.B. All-Solid-Thin Film Electrochromic Devices Consisting of Layers ITO/NiO/ZrO2/WO3/ITO. *J. Nano-Electron. Phys.* **2013**, *5*, 02023(3pp).
2. Granqvist, C.G. *Sol. Energ. Mat. Sol. Cells* **2000**, *60*, 201.
3. Lee, W.; Fang, Y.; Ho, J.J.; Hsieh, W.; Ting, S.; Huang, D.; Ho, F.C. Effects of surface porosity on tungsten trioxide(WO3) filmsâ€™ electrochromic performance. *J. Electron. Mater.* **2000**, *29*, 183–187. doi:10.1007/s11664-000-0139-8.
4. Habazaki, H.; Hayashi, Y.; Konno, H. *Elektrochim. Acta* **2002**, *47*, 4181.
5. Williams, D.E.; Aliwell, S.R.; Pratt, Keith F. E.; Caruana, D.J.; Jones, R.L.; Cox, R.A.; Hansford, G.M.; Halsall, J. Modelling the response of a tungsten oxide semiconductor as a gas sensor for the measurement of ozone. *Meas. Sci. Technol.* **2002**, *13*, 923–931.
6. Cantalini, C.; Sun, H.T.; Faccio, M.; Pelino, M.; Santucci, S.; Lozzi, L.; Passacantando, M. *Sensors Actuat. B* **1996**, *31*, 81.
7. Berak, J.M.; Sienko, M. J. Effect of oxygen–deficiency on electrical transport properties of tungsten trioxide crystals. *J. Solid State Chem.* **1970**, *2*, 109–133. doi:http://dx.doi.org/10.1016/0022-4596(70)90040-X.
8. Wiltner, A. Untersuchungen zur Diffusion und Reaktion von Kohlenstoff auf Nickel- und Eisenoberflächen sowie von Beryllium auf Wolfram. PhD thesis, Universität Bayreuth, 2005.
9. Miller, S.; Berning, G.L.P.; Plank, H.; Roth, J. X–ray photoelectron spectroscopy study of TiC films grown by annealing thin Ti films on graphite. *J. Vac. Sci. Technol. A* **1997**, *15*, 2029–2034.
10. Miller, S. Untersuchung der chemischen Wechselwirkung von Titan und Kohlenstoff mittels Röntgen-Photoelektronen-Spektroskopie. PhD thesis, Universität Bayreuth, 1997.
11. Physical Electronics. *MultiPak 6.1A*, 1999.
12. Briggs, D.; Grant, J.T., Eds. *Surface Analysis by Auger and X–Ray Photoelectron Spectroscopy*; IM Publications, Chichester and SurfaceSpectra Limited, Manchester, 2003.
13. Briggs, D.; Seah, M.P., Eds. *Practical Surface Analysis — Volume 1: Auger and X–Ray Photoelectron Spectroscopy*; John Wiley & Sons, Chichester, 1990.
14. Doniach, S.; Šunjić, M. Many–electron singularity in X–ray photoemission and X–ray line spectra from metals. *J. Phys. C: Solid State* **1970**, *3*, 285–291.
15. Shirley, D.A. High–Resolution X-Ray Photoemission Spectrum of the Valence Bands of Gold. *Phys. Rev. B* **1972**, *5*, 4709–4714.

16. Mundy, J.N.; Rothman, S.J.; Lam, N.Q.; Hoff, H.A.; Nowicki, L.J. Self–diffusion in tungsten. *Phys. Rev. B* **1978**, *18*, 6566–6575.
17. Bussolotti, F.; Lozzi, L.; Passacantando, M.; La Rosa, S.; Santucci, S.; Ottaviano, L. Surface electronic properties of polycrystalline WO3 thin films: a study by core level and valence band photoemission. *Surf. Sci.* **2003**, *538*, 113–123.
18. Khyzhun, O. XPS, XES and XAS studies of the electronic structure of tungsten oxides. *J. Alloys Comp.* **2000**, *305*, 1–6.
19. Jeong, J.I.; Hong, J.H.; Moon, J.H.; Kang, J.S.; Fukuda, Y. X-ray photoemission studies of W 4f core levels of electrochromic HxWO3 films. *J. Appl. Phys.* **1996**, *79(12)*, 9343–9348.
20. Katrib, A.; Hemming, F.; Wehrer, P.; Hilaire, L.; Maire, G. The multi-surface structure and catalytic properties of partially reduced WO3, WO2 and WC + O2 or W + O2 as characterized by XPS. *J. Electron Spectrosc. Relat. Phenom.* **1995**, *76*, 195–200.
21. Moulder.; Stickle.; Sobol.; Bomben. *Handbook of X–Ray Photoelectron Spectroscopy*; Pelkin–Elmer Corporation, 1992.
22. Fleisch, T.H.; Zajac, G.W.; Schreiner, J.O.; Mains, G.J. An XPS study of the UV photoreduction of transition and noble metal oxides. *Appl. Surf. Sci.* **1986**, *26*, 488–497.
23. Salvati, L.; Makovsky, L.E.; Stencel, J.M.; Brown, F.R.; Hercules, D.M. Surface spectroscopic study of tungsten-alumina catalysts using x-ray photoelectron, ion scattering, and Raman spectroscopies. *J. Phys. Chem.* **1981**, *85*, 3700–3707.
24. Wagner, C.D. X–ray photoelectron spectroscopy with X–ray photons of higher energy. *J. Vac. Sci. Technol.* **1978**, *15*, 518–523.
25. Nefedov, V.I.; Salyn, Y.V. A comparison of different spectrometers and charge corrections used in X-ray photoelectron spectroscopy. *J. Electron Spectrosc. Relat. Phenom.* **1977**, *10*, 121–124.
26. Lopatin, S.I.; Semenov, G.A. Thermochemical Study of Gaseous Salts of Oxygen-containing Acids: VIII. Beryllium Molybdate and Tungstates. *Russ. J. Gen. Chem.* **2001**, *71*, 1220–1224.
27. Chupka, W.; Berkowitz, J.; Giese, C. Vaporization of Beryllium Oxide and Its Reaction with Tungsten. *J. Chem. Phys.* **1959**, *30*, 827–834.
28. Linsmeier, C.; Ertl, K.; Roth, J.; Wiltner, A.; Schmid, K.; Kost, F.; Bhattacharyya, S.; Baldwin, M.; Doerner, R. Binary beryllium–tungsten mixed materials. *J. Nucl. Mater.* **2007**, *363–365*, 1129–1137. doi:DOI: 10.1016/j.jnucmat.2007.01.224.
29. Wiltner, A.; Kost, F.; Lindig, S.; Linsmeier, C. Structural investigation of the Be–W intermetallic system. *Phys. Scr.* **2007**, *T128*, 133–136.
30. Wiltner, A.; Linsmeier, C. Surface alloying of thin beryllium films on tungsten. *New J. Phys.* **2006**, *8*, 1–11.
31. Wiltner, A.; Linsmeier, C. Formation of a surface alloy in the beryllium–tungsten system. *J. Nucl. Mater.* **2005**, pp. 951–955.
32. Goldstraß, P.; Klages, K.U.; Linsmeier, C. Surface reactions on beryllium after carbon vapour deposition and thermal treatment. *J. Nucl. Mater.* **2001**, *290-293*, 76–79.
33. Linsmeier, C.; Wanner, J. Reactions of oxygen atoms and molecules with Au, Be, and W surfaces. *Surf. Sci.* **2000**, *454–456*, 305–309.
34. Köppen, M. Untersuchung des ternären Systems Wolfram-Sauerstoff-Beryllium / Investigation of the ternary system tungsten–oxygen–beryllium (in German). Master's thesis, Technical University of Munich, 2008. doi:10.13140/RG.2.2.24776.62723.